Mon. Not. R. Astron. Soc. **351,** 18–30 (2004) doi:10.1111/j.1365-2966.2004.07773.x

A completely analytical family of dynamical models for spherical galaxies and bulges with a central black hole

Maarten Baes★ and Herwig Dejonghe
Sterrenkundig Observatorium, Universiteit Gent, Krijgslaan 281-S9, B-9000 Gent, Belgium

Accepted 2004 February 24. Received 2004 February 23; in original form 2004 January 26

ABSTRACT

We present a family of spherical models for elliptical galaxies and bulges consisting of a stellar component and a central black hole. All models in this family share the same stellar density profile, which has a steep central cusp. The gravitational potential of each model is a linear combination of the potential generated self-consistently by the stars and the potential of a central black hole. The relative importance of these two contributions is a free parameter in the models. Assuming an isotropic dynamical structure, almost all kinematical properties of these models can be calculated analytically. In particular, they form the first simple dynamical models for galaxies with a central black hole where the distribution function and differential energy distribution can be written completely in terms of elementary functions only. We also present various extensions of this family to models with anisotropic orbital structures. Also for these dynamical models, the distribution function and its moments can be expressed completely in terms of elementary functions.

This family is useful for a large range of applications, in particular to generate initial conditions for *N*-body and hydrodynamical simulations to model galactic nuclei with a central black hole.

Key words: black hole physics – stellar dynamics – celestial mechanics – galaxies: kinematics and dynamics – galaxies: structure.

1 INTRODUCTION

During the past few years, various numerical dynamical modelling techniques have been developed to construct accurate dynamical models for galaxies (Dejonghe 1989; Emsellem, Monnet & Bacon 1994; Rix et al. 1997; Gerhard et al. 1998; van der Marel et al. 1998; Cretton et al. 1999; Gebhardt et al. 2000a; Verolme & de Zeeuw 2002). The state-of-the-art techniques can handle various degrees of complexity such as the capability to include non-trivial geometries and higher-order kinematical information. Nevertheless, analytical models remain interesting and important for various reasons. They can provide a simple test-bed where various physical processes can be investigated, or where new modelling or data analysis techniques can be explored. Analytical models are particularly useful to generate the initial conditions for *N*-body, smoothed particle hydrodynamics (SPH) or Monte Carlo simulations. Most attention has been devoted to the construction of spherical self-consistent models, i.e. models in which the stars move in a potential generated completely by the stars themselves. Famous examples include the Plummer model (Plummer 1911; Dejonghe 1987), the isochrone sphere (Hénon 1959, 1960), the Jaffe sphere (Jaffe 1983) and the Hernquist model (Hernquist 1990; Baes & Dejonghe 2002). Such models often serve as a template model for elliptical galaxies, globular clusters or the bulges of spiral galaxies.

Recent observational evidence indicates, however, that the central regions of these stellar systems cannot always be faithfully represented by self-consistent models. The existence of supermassive black holes in the nuclei of galaxies has been suspected for a long time, as accretion on to massive compact objects was regarded as the only reasonable explanation for the existence of active galaxies and quasars (Salpeter 1964; Sołtan 1982). During the last decade, quiescent supermassive black holes have been detected in the centre of the Milky Way (Ghez et al. 2000; Schödel et al. 2002) and in the nuclei of virtually all external galaxies which are near enough to resolve the sphere of influence of the black hole (e.g. see the list in Tremaine et al. 2002). The masses of these black holes are roughly between a million and a few billion solar masses and are tightly coupled to structural parameters of the host galaxies (Kormendy & Richstone 1995; Ferrarese & Merritt 2000; Gebhardt et al. 2000b; Graham, Trujillo & Caon 2001; Ferrarese 2002; McLure & Dunlop 2002; Baes et al. 2003; Marconi & Hunt 2003).

★E-mail: maarten.baes@ugent.be

Recently, evidence for the presence of intermediate-mass black holes in the centre of globular clusters has been reported (Gebhardt, Rich & Ho 2002; Gerssen et al. 2002, 2003), although this evidence is still controversial (Baumgardt et al. 2003a,b; McNamara, Harrison & Anderson 2003). These observations clearly indicate that there is a need for simple but realistic analytical dynamical models with a central black hole.

The first requirement for the construction of models with a black hole is a potential–density pair with a cuspy central density profile. Tremaine et al. (1994) demonstrate that spherical isotropic systems need a central density profile that diverges at least as $r^{-1/2}$ to be able to support a central black hole. The need for such cuspy models also follows from observations: *Hubble Space Telescope* (*HST*) photometry has shown that ellipticals and the bulges of spiral galaxies generally have central density cusps that diverge as $r^{-\gamma}$ at small radii with $0 \leqslant \gamma \leqslant 2.5$ (Lauer et al. 1995; Gebhardt et al. 1996; Ravindranath et al. 2001; Seigar et al. 2002). Also for the Milky Way there is evidence for a central density cusp in the innermost regions (Genzel et al. 2003). A very useful one-parameter family of spherical models with this characteristic, which we refer to as the γ-models, was introduced independently by Dehnen (1993) and Tremaine et al. (1994). This family has a simple analytical density profile which diverges as $r^{-\gamma}$ in the central regions ($0 \leqslant \gamma < 3$), and includes the Hernquist and Jaffe models as special cases. Zhao (1996) generalized this family further to a very general three-parameter family of models, the so-called (α, β, γ)-models. For many of these models, interesting dynamical properties such as the intrinsic and projected velocity dispersions, the distribution function and the differential energy distribution can be calculated analytically if one assumes an isotropic self-consistent dynamical structure.

The second step in the construction of dynamical models with a cuspy core is to add to the potential of the self-consistent model an extra contribution from the black hole, and recalculate the dynamical properties with this new potential. The calculation of the (intrinsic and/or projected) velocity dispersions in the presence of a black hole is not very difficult, and can usually be performed analytically for those models where the dispersions can be calculated analytically in the self-consistent case. For example, for the sets of potential–density pairs considered by Tremaine et al. (1994) and Zhao (1996), the addition of a black hole was not a problem for the calculation of the velocity dispersion profile. The reason is that the intrinsic and projected velocity dispersions are just linear functions of the potential, and therefore linear functions of the black hole mass. Many other interesting kinematical properties, in particular the phase space distribution function, depend on the potential in a strongly non-linear way, however. The construction of dynamical models in which these more complicated kinematical quantities can be expressed analytically in the presence of a black hole proves to be more difficult. Apart from the asymptotic behaviour, these characteristics usually need to be calculated numerically (Tremaine et al. 1994; Dejonghe et al. 1999).

The work by Ciotti (1996) provides a first attempt to construct completely analytical dynamical models for galaxies with a central black hole. In an effort to construct realistic dynamical models for elliptical galaxies embedded in massive cuspy dark matter haloes, he considers a set of two-component Hernquist models. They consist of a stellar component and a halo component, both of which are modelled as a Hernquist profile, but with different masses and core radii. The interesting aspect of his work for our goal is that the masses and core radii of each component can be taken arbitrarily. Setting the core radius of the halo component to zero, his two-component model degenerates into a Hernquist model with a central black hole. Ciotti demonstrates that the distribution function and differential energy distribution of Hernquist models with a central black hole can be expressed analytically, albeit as rather cumbersome expressions. For example, the distribution function can be written as the derivative of a complicated function involving incomplete elliptic integrals and Jacobian functions. Nevertheless, his work presents the first model for galaxies with a central black hole where most of the kinematical properties can be calculated analytically.

In this paper, we present a detailed kinematical analysis of a family of spherical models for elliptical galaxies and bulges consisting of a stellar component and a central black hole. In Section 2 we define our family of models. All models in this one-parameter family share the same stellar density profile, which corresponds to one of the γ-models introduced by Dehnen (1993) and Tremaine et al. (1994). The potential of the models is a linear combination of the potential generated by the stars and the potential of a central black hole. The importance of both components to the total potential can be set arbitrarily by varying the parameter μ, which represents the mass of the central black hole relative to the total mass. The reason why we chose this particular family of models is that most of the interesting kinematical properties can be expressed completely analytically for all values of μ. In Section 3 we describe some intrinsic kinematical properties of this family of models, such as the distribution function, the differential energy distribution and the moments of the distribution function. In particular, we give closed analytical expressions for these quantities, completely in terms of elementary functions. In Section 4 we describe some observed kinematical properties as they are projected on the plane of the sky. Most of these quantities can be expressed analytically involving simple incomplete elliptic integrals. In Section 5 we present a number of generalizations to models with an anisotropic orbital structure. In particular, we discuss models with a constant anisotropy profile, models with a distribution function of the Osipkov–Merritt type and models with a completely radial orbital structure. Also for these models, the distribution function and its moments can be calculated completely analytically for all values of the central black hole mass. Finally, a discussion is given in Section 6.

2 DEFINITION OF THE MODELS

The starting point for our family of models is the stellar luminosity density profile

$$\rho(r) = \frac{L_\star}{8\pi}\left(\frac{r}{c}\right)^{-5/2}\left(1+\frac{r}{c}\right)^{-3/2}, \tag{1}$$

where $L_\star$ is the total stellar luminosity of the system and c is a scalelength. The (positive) potential generated by this stellar distribution is easily found through Poisson's equation,

$$\Psi_\star(r) = -\Phi_\star(r) = \frac{2GM_\star}{c}\left(\sqrt{\frac{r+c}{r}} - 1\right), \tag{2}$$

where $M_\star$ is the total stellar mass. The isotropic self-consistent model with this potential–density pair is a particular case from the family of γ-models considered by Dehnen (1993) and Tremaine et al. (1994), corresponding to $\gamma = 5/2$ or $\eta = 1/2$. A number of kinematical properties for this self-consistent model, such as the velocity dispersion and distribution function, has been derived in these papers. Our aim is to consider systems consisting of two components: a stellar component and a central supermassive black hole. In order to find the total potential of such a two-component system, we need to add to the stellar potential an extra contribution from the black hole. We model the central black hole as a point potential with mass $M_\bullet$, such that we obtain

$$\Psi(r) = \frac{2GM_\star}{c}\left(\sqrt{\frac{r+c}{r}} - 1\right) + \frac{GM_\bullet}{r}. \tag{3}$$

In the remainder of this paper, we will work in dimensionless units: we set the gravitational constant G, the scalelength c, the luminosity $L_\star$ and the *total* mass $M_\star + M_\bullet$ of the model equal to unity. We introduce the parameter μ as the fraction of the black hole mass to the total mass of the galaxy. With these conventions, we can write the potential–density pair of our model as

$$\rho(r) = \frac{1}{8\pi}\frac{1}{r^{5/2}(1+r)^{3/2}}, \tag{4}$$

$$\Psi(r) = 2(1-\mu)\left(\sqrt{\frac{1+r}{r}} - 1\right) + \frac{\mu}{r}. \tag{5}$$

In this paper, we consider isotropic kinematical models implied by the potential–density pair formed by equations (4) and (5). This potential–density pair defines a one-parameter family of isotropic dynamical models, where μ is a free parameter that can assume any value between 0 and 1. The models corresponding to these values of μ have a particular meaning: the former corresponds to a self-consistent model without a central black hole, whereas the latter represents a galaxy with a central black hole and a negligible stellar mass-to-light ratio.

As an important remark, the reader should note that the convention we use is different from the convention used in, e.g. Tremaine et al. (1994) and Zhao (1996). In these papers, μ denotes the black hole mass relative to the *stellar* mass, and the normalization is such that the stellar mass is set to unity. We prefer to set the *total* mass of the galaxy equal to unity, however, because (1) all models then have the same behaviour at large radii and (2) this allows us to study the entire range of models from self-consistent models without a black hole to models completely dominated by the black hole potential.

3 INTRINSIC PROPERTIES OF THE MODELS

3.1 Basic properties

The total mass density, circular velocity curve and the cumulative mass function are readily obtained

$$\rho_{\rm tot}(r) = \frac{1-\mu}{8\pi}\frac{1}{r^{5/2}(1+r)^{3/2}} + \mu\delta(\boldsymbol{r}), \tag{6}$$

$$v_{\rm c}^2(r) = \frac{1-\mu}{\sqrt{r(1+r)}} + \frac{\mu}{r}, \tag{7}$$

$$M(r) = (1-\mu)\sqrt{\frac{r}{1+r}} + \mu. \tag{8}$$

The isotropic velocity dispersion $\sigma = \sigma_r = \sigma_\theta = \sigma_\phi$ can be obtained from the solution of the Jeans equation,

$$\sigma^2(r) = \frac{1}{\rho(r)}\int_r^\infty \frac{M(r)\rho(r)\mathrm{d}r}{r^2}. \tag{9}$$

The cumulative mass function, which depends linearly on the black hole mass, is the only μ-dependent quantity in this expression. Consequently we can write the velocity dispersion as the sum of separate contributions from the stellar mass and the black hole. The result is

$$\sigma^2(r) = \frac{1-\mu}{3}\sqrt{\frac{1+r}{r}}\left[1 - 2r + 6r^2 + 12r^3 - 12r^3(1+r)\ln\left(\frac{1+r}{r}\right)\right] + \frac{2\mu}{35}\left(\frac{1+r}{r}\right)\left(5 - 8r + 16r^2 - 64r^3 - 128r^4 + 128r^{7/2}\sqrt{1+r}\right). \tag{10}$$

At large radii, the velocity dispersion goes to zero as

$$\sigma^2(r) \approx \frac{1}{5r}\left(1 - \frac{2-5\mu}{12r} + \cdots\right). \tag{11}$$

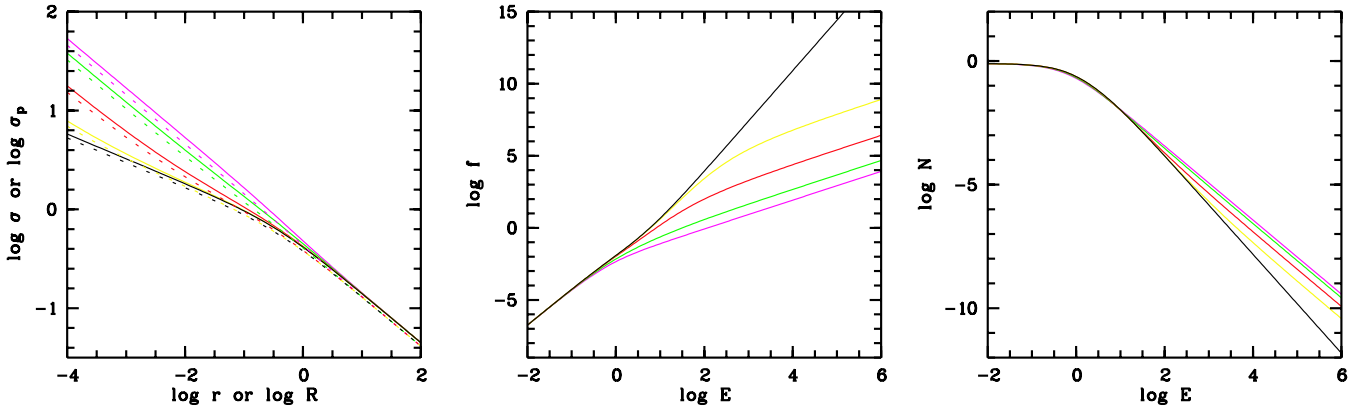

Figure 1. Some intrinsic and projected kinematical properties of the model for various values of the parameter μ. The first panel shows the intrinsic velocity dispersion profile $\sigma(r)$ [solid lines] and the projected velocity dispersion profile $\sigma_{\rm p}(R)$ [dotted lines], the second panel shows the distribution function $f(\mathcal{E})$ and in the right panel the differential energy distribution $\mathcal{N}(\mathcal{E})$ is plotted. The colour code is the same for all panels: $\mu = 0$ (black), $\mu = 0.01$ (yellow), $\mu = 0.1$ (red), $\mu = 0.5$ (green) and $\mu = 1$ (magenta).

At small radii, the velocity dispersion diverges as

$$\sigma^2(r) \approx \frac{1-\mu}{3\sqrt{r}}\left(1-\frac{3r}{5}+\cdots\right)+\frac{2\mu}{7r}\left(1-\frac{3r}{2}+\cdots\right). \tag{12}$$

In the left panel of Fig. 1 we plot the intrinsic velocity dispersion profile for various black hole masses. Without a central black hole, the velocity dispersion (and the circular velocity) have a weak $r^{-1/4}$ divergence at small radii. When a black hole is present, these divergences become stronger and both quantities diverge as $r^{-1/2}$.

3.2 The distribution function

The ultimate goal of the dynamical modeller is to obtain an expression for the phase-space distribution function $f(\boldsymbol{r}, \boldsymbol{v})$, which contains all kinematical information on a system. For non-rotating isotropic spherically symmetric systems, the phase-space distribution function depends on the position and velocity vectors only through the binding energy $\mathcal{E} = \psi(r) - \frac{1}{2}\boldsymbol{v}^2$, which is an integral of the motion. The distribution function $f(\boldsymbol{r}, \boldsymbol{v}) = f(\mathcal{E})$ is thus a one-dimensional rather than a six-dimensional function. The key to calculating the distribution function corresponding to a given potential–density pair is the augmented density $\tilde{\rho}(\Psi)$, i.e. the density written in terms of the potential. With this function, we can calculate the distribution function through the Eddington (1916) relation,

$$f(\mathcal{E}) = \frac{1}{\sqrt{8}\pi^2}\left[\int_0^{\mathcal{E}}\frac{{\rm d}^2\tilde{\rho}}{{\rm d}\Psi^2}\frac{{\rm d}\Psi}{\sqrt{\mathcal{E}-\Psi}}+\frac{1}{\sqrt{\mathcal{E}}}\left(\frac{{\rm d}\tilde{\rho}}{{\rm d}\Psi}\right)_{\Psi=0}\right]. \tag{13}$$

The second term in this expression vanishes for the family of models we consider in this paper, both with and without a black hole, because $\tilde{\rho}(\Psi) \propto \Psi^4$ at large radii. To find an expression for the augmented density, we need to invert the potential to a relation $r(\Psi)$ and determine $\tilde{\rho}(\Psi) = \rho(r(\Psi))$.

We first consider the special case when the galaxy contains no central black hole ($\mu = 0$). The augmented density is readily found,

$$\tilde{\rho}(\Psi) = \frac{1}{256\pi}\frac{\Psi^4(4+\Psi)^4}{(2+\Psi)^3}, \tag{14}$$

and the resulting distribution function is (Tremaine et al. 1994)

$$f(\mathcal{E}) = \frac{\sqrt{2}}{896\pi^3}\left[\frac{42(3-32\mathcal{E}-8\mathcal{E}^2)}{(2+\mathcal{E})^{9/2}}\,\mathrm{arcsinh}\sqrt{\frac{\mathcal{E}}{2}} - \frac{(63-693\mathcal{E}-5670\mathcal{E}^2-7410\mathcal{E}^3-4488\mathcal{E}^4-1448\mathcal{E}^5-240\mathcal{E}^6-16\mathcal{E}^7)\sqrt{\mathcal{E}}}{(2+\mathcal{E})^4}\right]. \tag{15}$$

The behaviour at small binding energies is

$$f(\mathcal{E}) \approx \frac{2\sqrt{2}}{5\pi^3}\mathcal{E}^{5/2}\left(1-\frac{5\mathcal{E}}{7}+\cdots\right), \tag{16}$$

whereas at large binding energies we obtain

$$f(\mathcal{E}) \approx \frac{\sqrt{2}}{56\pi^3}\mathcal{E}^{7/2}\left(1+\frac{7}{\mathcal{E}}+\cdots\right). \tag{17}$$

Another special case is the other side of the spectrum ($\mu = 1$), which corresponds to a galaxy where the black hole completely dominates the potential. In this case the augmented density and distribution function read

$$\tilde{\rho}(\Psi) = \frac{1}{8\pi}\frac{\Psi^4}{(1+\Psi)^{3/2}}, \tag{18}$$

$$f(\mathcal{E}) = \frac{\sqrt{2}}{128\pi^3}\left[\frac{(9+9\mathcal{E}+31\mathcal{E}^2+15\mathcal{E}^3)\sqrt{\mathcal{E}}}{(1+\mathcal{E})^3} - 3\,(3-5\mathcal{E})\arctan\sqrt{\mathcal{E}}\right]. \tag{19}$$

The behaviour at small binding energies is

$$f(\mathcal{E}) \approx \frac{2\sqrt{2}}{5\pi^3}\mathcal{E}^{5/2}\left(1 - \frac{15\mathcal{E}}{7} + \cdots\right), \tag{20}$$

whereas at large binding energies we obtain

$$f(\mathcal{E}) \approx \frac{15\sqrt{2}}{256\pi^2}\mathcal{E}\left(1 - \frac{3}{5\mathcal{E}} + \cdots\right). \tag{21}$$

For the general case $0 < \mu < 1$, i.e. when both the stars and the central black hole contribute to the potential of the galaxy, the calculation of the distribution function is more tedious. In order to find a convenient expression for the augmented density, we write expression (4) as

$$\rho(a) = \frac{1}{8\pi}\frac{(a^2-1)^4}{a^3} \qquad \text{with} \qquad a \equiv a(r) = \sqrt{\frac{1+r}{r}}. \tag{22}$$

A relation $a(\Psi)$ can be found by inverting the expression

$$\Psi(a) = 2\,(1-\mu)\,(a-1) + \mu(a^2-1), \tag{23}$$

which yields

$$a(\Psi) = \frac{\mu - 1 + \sqrt{1+\mu\Psi}}{\mu}. \tag{24}$$

To calculate a closed expression for the distribution function, we can now take different approaches. The first approach is a direct application of the Eddington formula (13). When we substitute the explicit expression for $a(\Psi)$ into the formula (22), we find after some algebra that the second derivative of the augmented density can be written in the form

$$\frac{\mathrm{d}^2\tilde{\rho}}{\mathrm{d}\Psi^2}(\Psi) = \frac{1}{32\pi\mu^3(2-\mu+\Psi)^5}\left[P_1(\Psi,\mu) + \frac{P_2(\Psi,\mu)}{(1+\mu\Psi)^{3/2}}\right], \tag{25}$$

where P_1 and P_2 are polynomials with integer coefficients in Ψ and μ. This form is suitable for analytical integration in the Eddington relation: the two parts of the integrand are basically the combination of a rational function of Ψ and the square root of first- and second-order polynomials in Ψ. Such a function can be integrated analytically and the resulting integral can be written in terms of elementary functions only. The distribution function can also be calculated in a more elegant way by transforming the Eddington relation (13) to an integration with respect to a. We obtain

$$f(\mathcal{E}) = \frac{1}{\sqrt{8}\pi^2}\int_1^{a_\mathcal{E}} \frac{\mathrm{d}}{\mathrm{d}a}\left[\frac{\mathrm{d}\tilde{\rho}}{\mathrm{d}a}\Big/\frac{\mathrm{d}\Psi}{\mathrm{d}a}\right]\frac{\mathrm{d}a}{\sqrt{\mathcal{E}-2(1-\mu)(a-1)-\mu(a^2-1)}} \tag{26}$$

with

$$a_\mathcal{E} = \frac{\mu - 1 + \sqrt{1+\mu\mathcal{E}}}{\mu}. \tag{27}$$

With the expressions (22) and (23) the first factor in the integrand becomes

$$\frac{\mathrm{d}}{\mathrm{d}a}\left[\frac{\mathrm{d}\tilde{\rho}}{\mathrm{d}a}\Big/\frac{\mathrm{d}\Psi}{\mathrm{d}a}\right] = \frac{1}{16\pi}\frac{(a^2-1)^2[12(1-\mu)+15\mu a+16(1-\mu)a^2+18\mu a^3+20(1-\mu)a^4+15\mu a^5]}{a^5(1-\mu+\mu a)^2}. \tag{28}$$

This function can be decomposed in partial fractions, and each of the resulting integrals can be calculated analytically in terms of elementary functions. Using either of these approaches, we obtain that the resulting distribution function can be written explicitly as

$$\begin{aligned} f(\mathcal{E}) = \frac{\sqrt{2}}{128\pi^3}\Bigg[&-\frac{\mathcal{X}(\mathcal{E},\mu)\sqrt{\mathcal{E}}}{\mu^3(2-\mu+\mathcal{E})^4(1+\mu\mathcal{E})} + \frac{3(25-40\mu+12\mu^2+5\mu\mathcal{E})}{\mu^{7/2}}\arctan\sqrt{\mu\mathcal{E}} \\ &+\frac{3(1-\mu)(3-8\mu+12\mu^2-32\mathcal{E}-31\mu\mathcal{E}-8\mathcal{E}^2)}{(2-\mu+\mathcal{E})^{9/2}}\operatorname{arctanh}\left(\frac{\sqrt{(2-\mu+\mathcal{E})\mathcal{E}}}{1+\mathcal{E}}\right)\Bigg], \end{aligned} \tag{29}$$

where $\mathcal{X}(\mathcal{E},\mu)$ is a polynomial with integer coefficients

$$\begin{aligned} \mathcal{X}(\mathcal{E},\mu) = {}& 3(400-1440\mu+2072\mu^2-1541\mu^3+622\mu^4-116\mu^5) \\ &+(2400-6400\mu-5352\mu^2-503\mu^3-1658\mu^4+1002\mu^5+220\mu^6)\mathcal{E} \\ &+(1800-2600\mu-1486\mu^2+4030\mu^3-2175\mu^4+373\mu^5)\mathcal{E}^2+2(300+150\mu-1356\mu^2+1116\mu^3-253\mu^4)\mathcal{E}^3 \\ &+(75+400\mu-864\mu^2+328\mu^3)\mathcal{E}^4+5\mu(13-16\mu)\mathcal{E}^5. \end{aligned} \tag{30}$$

The first two terms in the distribution function (29) both diverge as μ^{-3} when μ approaches zero, but the diverging terms of course cancel out, such that the distribution function reduces to the expression (15) in the limit $\mu \to 0$, as required. On the other hand, it is straightforward to check that the distribution function (29) reduces to the expression (19) in the limit $\mu \to 1$. At small binding energies, the distribution function (29) behaves as

$$f(\mathcal{E}) \approx \frac{2\sqrt{2}}{5\pi^3}\mathcal{E}^{5/2}\left[1 - \frac{5(1+2\mu)\mathcal{E}}{7} + \cdots\right], \tag{31}$$

and at large binding energies we have the expansion

$$f(\mathcal{E}) \approx \frac{15\sqrt{2}}{256\pi^2}\frac{\mathcal{E}}{\mu^{5/2}}\left[1 - \frac{32(1-\mu)}{3\pi\sqrt{\mu}\sqrt{\mathcal{E}}} + \frac{25 - 40\mu + 12\mu^2}{5\mu\mathcal{E}} + \cdots\right]. \tag{32}$$

In the second panel of Fig. 1 we plot the distribution function for different values of the black hole mass. As the central potential well is infinitely deep, orbits with all binding energies are allowed. Both without and with a central black hole, the distribution function is a monotonically rising function, which guarantees the stability of the model against radial and non-radial perturbations. At small binding energies the influence of a black hole is negligible. This is also visible in the asymptotic expansion (31), where the leading term is independent of the black hole mass fraction μ. The same leading terms are then obviously found in the asymptotic expansions (16) and (20). At large binding energies, i.e. in the central regions of the system, the influence of the black hole is important. The distribution function becomes less steep in the large binding energy limit when a black hole is present: its slope changes from 7/2 to 1. The larger the black hole mass, the smaller the values of the distribution function.

3.3 The differential energy distribution

The distribution function $f(\boldsymbol{r}, \boldsymbol{v}) = f(\mathcal{E})$ contains all available kinematical information on the system, but is rather hard to interpret. In particular, $f(\mathcal{E})$ does not represent the number of stars per unit binding energy. The quantity that describes this useful characteristic is the differential energy distribution $\mathcal{N}(\mathcal{E})$. For an isotropic spherical system, the differential energy distribution can be written as $\mathcal{N}(\mathcal{E}) = f(\mathcal{E})g(\mathcal{E})$, where $g(\mathcal{E})$ is called the density of states and represents the phase-space volume per unit binding energy (Binney & Tremaine 1987). This function can be calculated through the equation

$$g(\mathcal{E}) = 16\sqrt{2}\pi^2 \int_{\mathcal{E}}^{\infty} \left| r^2 \frac{\mathrm{d}r}{\mathrm{d}\Psi} \right| \sqrt{\Psi - \mathcal{E}}\, \mathrm{d}\Psi. \tag{33}$$

For the self-consistent model without a black hole, the density of states can immediately be calculated

$$g(\mathcal{E}) = \sqrt{2}\pi^3 \left[\frac{1 - \mathcal{E} + \mathcal{E}^2}{\mathcal{E}^{5/2}} - \frac{21 + 9\mathcal{E} + \mathcal{E}^2}{(\mathcal{E}+4)^{5/2}}\right], \tag{34}$$

and the differential energy distribution is found by multiplying this expression by the distribution function (15). At small binding energies, the differential energy distribution asymptotically behaves as

$$\mathcal{N}(\mathcal{E}) \approx \frac{4}{5}\left(1 - \frac{12\mathcal{E}}{7} + \cdots\right), \tag{35}$$

and at large binding energies we have the expansion

$$\mathcal{N}(\mathcal{E}) \approx \frac{3}{2\mathcal{E}^2}\left(1 - \frac{4}{\mathcal{E}} + \cdots\right). \tag{36}$$

If the potential of the galaxy is completely dominated by the black hole, we obtain the well-known and very simple expression for the density of states function,

$$g(\mathcal{E}) = \frac{\sqrt{2}\pi^3}{\mathcal{E}^{5/2}}. \tag{37}$$

Combining this expression with equation (19) for the distribution function, we find that the differential energy distribution asymptotically behaves as

$$\mathcal{N}(\mathcal{E}) \approx \frac{4}{5}\left(1 - \frac{15\mathcal{E}}{7} + \cdots\right), \tag{38}$$

in the small binding energy limit, whereas at large binding energies we have the asymptotic expansion

$$\mathcal{N}(\mathcal{E}) \approx \frac{15\pi}{128\mathcal{E}^{3/2}}\left(1 - \frac{3}{5\mathcal{E}} + \cdots\right). \tag{39}$$

In the general case $0 < \mu < 1$, the calculation of the density of states is less straightforward. Similarly as for the distribution function, we have calculated the function $g(\mathcal{E})$ in two ways. The first approach uses a brute-force calculation of the definition (33). A more subtle approach consists of transforming the integral in this expression to an integration with respect to a. We obtain

$$g(\mathcal{E}) = 32\sqrt{2}\pi^2 \int_{a_{\mathcal{E}}}^{\infty} \frac{a}{(a^2-1)^4} \sqrt{2(1-\mu)(a-1) + \mu(a^2-1) - \mathcal{E}}\, \mathrm{d}a, \tag{40}$$

with $a_{\mathcal{E}}$ as in equation (27). This integral can be calculated analytically and results in

$$g(\mathcal{E}) = \sqrt{2}\pi^2 \left\{ \frac{2(1-\mu)\left[24(1-\mu) - 4(3-10\mu+4\mu^2)\mathcal{E} - 2(9-11\mu)\mathcal{E}^2 - 3\mathcal{E}^3\right]\sqrt{\mu}}{3\mathcal{E}^2(4-4\mu+\mathcal{E})^2} \right.$$
$$- \frac{1-(1-\mu)\mathcal{E}+(1-\mu)\mathcal{E}^2}{\mathcal{E}^{5/2}}\left[\pi - \arctan\sqrt{\mu\mathcal{E}}\right]$$
$$\left. + \frac{(21-70\mu+80\mu^2-32\mu^3)+(9-19\mu+10\mu^2)\mathcal{E}+(1-\mu)\mathcal{E}^2}{(4-4\mu+\mathcal{E})^{5/2}}\left[\arctan\left(\frac{2\mu-1}{\sqrt{\mu(4-4\mu+\mathcal{E})}}\right) - \frac{\pi}{2}\right]\right\}. \tag{41}$$

In the limits $\mu \to 0$ and $\mu \to 1$, this function reduces to the expressions (34) and (37) respectively. The differential energy distribution $\mathcal{N}(\mathcal{E})$ of the model we consider can thus be written completely in terms of elementary functions for all values of μ. At small binding energies, the differential energy distribution behaves as

$$\mathcal{N}(\mathcal{E}) \approx \frac{4}{5}\left[1 - \frac{3(4+\mu)\mathcal{E}}{7} + \cdots\right], \tag{42}$$

and at large binding energies we find the expansion

$$\mathcal{N}(\mathcal{E}) \approx \frac{15\pi\sqrt{\mu}}{128\mathcal{E}^{3/2}}\left[1 + \frac{32(1-\mu)}{5\pi\sqrt{\mu}}\frac{1}{\sqrt{\mathcal{E}}} + \left(\frac{100-215\mu+112\mu^2}{5\mu} - \frac{8192(1-\mu)^2}{45\pi^2\mu}\right)\frac{1}{\mathcal{E}} + \cdots\right]. \tag{43}$$

In the right-hand panel of Fig. 1 we plot the differential energy distribution for models with various black hole masses. Without a black hole, the differential energy distribution is a monotonically decreasing function that has a finite value at $\mathcal{E} = 0$ and that decreases smoothly to zero as $\mathcal{E}^{-2}$ at large binding energies. In spite of the strong divergence of the distribution function at large binding energies, the system thus has no stars at rest in the centre of the galaxy. Both of these properties (a finite value at $\mathcal{E} = 0$ and convergence to zero at large $\mathcal{E}$) are common properties for all self-consistent models in the family of γ-models (Dehnen 1993). Adding a supermassive black hole does not change the behaviour of the differential energy distribution very drastically. The differential energy distribution still reaches the same finite value 4/5 at $\mathcal{E} = 0$, and then smoothly decreases for increasing binding energies. The slope of the differential energy distribution is a weakly decreasing function of μ. At large binding energies, the differential energy distribution still converges to zero, but the slope of the convergence is weakened from -2 to $-3/2$. For increasing black hole mass, the differential energy distribution assumes smaller values at small binding energies and converges less rapidly to zero at large binding energies. Models with increasing black hole masses hence contain stars which are in the mean increasingly strongly bound to the galaxy.

3.4 The moments of the distribution function

It is useful to consider the moments of the distribution function with respect to the velocities. In a general non-rotating spherical system, the moments of the distribution function are defined as

$$\mu_{2i,2j,2k}(r) = \iiint f(r,\boldsymbol{v}) v_r^{2i} v_\theta^{2j} v_\phi^{2k}\,\mathrm{d}\boldsymbol{v}, \tag{44}$$

where the integration covers the entire velocity space. For isotropic spherical systems the distribution function is symmetric in the velocities, and one defines the isotropic moments as

$$\mu_{2n}(r) = 4\pi\int_0^{\sqrt{2\Psi(r)}} f(r,v) v^{2n+2}\,\mathrm{d}v. \tag{45}$$

It is easily shown that the relation between the general moments and the isotropic moments is

$$\mu_{2i,2j,2k}(r) = \frac{1}{2\pi}\frac{\Gamma\left(i+\frac{1}{2}\right)\Gamma\left(j+\frac{1}{2}\right)\Gamma\left(k+\frac{1}{2}\right)}{\Gamma\left(i+j+k+\frac{3}{2}\right)}\mu_{2(i+j+k)}(r). \tag{46}$$

Knowledge of the isotropic moments is thus sufficient to determine all the moments. A direct integration of the definition is not the most obvious way to calculate the moments. A more interesting way is to use a formula that expresses the augmented moments, i.e. the moments written as a function of the potential, as a function of the augmented density (Dejonghe 1986),

$$\tilde{\mu}_{2n}(\Psi) = \frac{(2n+1)!!}{(n-1)!!}\int_0^\Psi \left(\Psi - \Psi'\right)^{n-1}\tilde{\rho}\left(\Psi'\right)\,\mathrm{d}\Psi'. \tag{47}$$

For the model we consider, we can write this expression as

$$\tilde{\mu}_{2n}(\Psi) \equiv \tilde{\mu}_{2n}(a) = \frac{1}{4\pi}\frac{(2n+1)!!}{(n-1)!!}\int_1^a \frac{\left(1-a'^2\right)^4(1-\mu+\mu a')}{a'^3}\left[2(1-\mu)\left(a-a'\right)+\mu\left(a^2-a'^2\right)\right]^{n-1}\,\mathrm{d}a'. \tag{48}$$

For all integer values of n, the integrand of this integral is a simple power series in a' and can easily be integrated analytically. The $2n$-th moment can be written as a polynomial in μ of order n, where each coefficient is a sum of powers in a and terms in $\ln a$. The true isotropic moments $\mu_{2n}(r)$ can subsequently be found by substitution of $a = \sqrt{(1+r)/r}$ into the result. For example, for the second-order moment,

one obtains

$$\tilde{\mu}_2(a) = \frac{3}{\pi}\left[(1-\mu)\left(-\frac{1}{8a^2}-\frac{5}{12}-\ln a+\frac{3a^2}{4}-\frac{a^4}{4}+\frac{a^6}{24}\right)+\mu\left(-\frac{1}{a}+\frac{32}{35}-a+\frac{a^3}{2}-\frac{a^5}{5}+\frac{a^7}{28}\right)\right]. \tag{49}$$

If we substitute $a=\sqrt{(1+r)/r}$ and $\mu_2 = 3\rho\sigma^2$ into this equation, we recover the expression (10).

4 OBSERVED PROPERTIES OF THE MODEL

4.1 The surface brightness

The surface brightness profile can be found by projecting the luminosity density profile on the plane of the sky,

$$I(R) = 2\int_R^\infty \frac{\rho(r) r\,\mathrm{d}r}{\sqrt{r^2-R^2}}. \tag{50}$$

As all models in the family we investigate share the same stellar density profile, they will obviously share the same surface brightness profile. This can be written in terms of incomplete elliptic integrals of the first and second kind,

$$I(R) = \frac{1}{\pi}\left[\frac{1}{2(1-R^2)}+\frac{R^2-\frac{1}{2}}{R^{3/2}(R-1)\sqrt{R+1}}\mathbb{E}\left(\frac{\pi}{4},\sqrt{\frac{2}{R+1}}\right)-\frac{1}{\sqrt{R(R+1)}}\mathbb{F}\left(\frac{\pi}{4},\sqrt{\frac{2}{R+1}}\right)\right]. \tag{51}$$

In the appendix we give the relevant formulae to transform this formula (and similar formulae which will appear in the remainder of this discussion) into a more convenient form for $R<1$ and $R\approx 1$. At large projected radii, the surface brightness decreases as

$$I(R) \approx \frac{1}{16R^3}\left(1-\frac{4}{\pi R}+\cdots\right), \tag{52}$$

and the behaviour at small projected radii is

$$I(R) \approx \sqrt{\frac{\pi}{2}}\frac{1}{\Gamma^2}R^{-3/2}\left(1-\frac{3\Gamma^4}{16\pi^2}R+\cdots\right), \tag{53}$$

where $\Gamma \equiv \Gamma(1/4)\approx 3.62561$. The cumulative surface brightness profile can be found by integrating the surface density over a circular surface on the plane of the sky,

$$S(R) = 2\pi\int_0^R I(R')R'\,\mathrm{d}R'. \tag{54}$$

A more convenient expression can be found by substitution of the definition (50) into this expression and partial integration,

$$S(R) = 1-4\pi\int_R^\infty \rho(r)\sqrt{r^2-R^2}\,r\,\mathrm{d}r. \tag{55}$$

For the luminosity density profile we consider, this expression can also be written in terms of incomplete elliptic integrals of the first and second kind

$$S(R) = 2\sqrt{R(R+1)}\,\mathbb{E}\left(\frac{\pi}{4},\sqrt{\frac{2}{R+1}}\right)-\frac{2R^{3/2}}{\sqrt{R+1}}\mathbb{F}\left(\frac{\pi}{4},\sqrt{\frac{2}{R+1}}\right). \tag{56}$$

The effective radius $R_{\rm eff}$ is obtained by solving the equation $S(R_{\rm eff})=1/2$; a numerical evaluation gives $R_{\rm eff}=0.244\,955$.

4.2 The projected velocity dispersion

The projected velocity dispersion can be found by projecting the intrinsic velocity dispersion profile on the plane of the sky,

$$\sigma_{\rm p}^2(R) = \frac{2}{I(R)}\int_R^\infty \frac{\rho(r)\sigma^2(r) r\,\mathrm{d}r}{\sqrt{r^2-R^2}}, \tag{57}$$

or after substitution of the Jeans solution (9) and partial integration,

$$\sigma_{\rm p}^2(R) = \frac{2}{I(R)}\int_R^\infty \frac{\rho(r)M(r)\sqrt{r^2-R^2}\,\mathrm{d}r}{r^2}. \tag{58}$$

Similarly as for the intrinsic dispersion, we can write the projected velocity dispersion as the sum of separate contributions from the stellar mass and the black hole. The contribution of the stellar mass leads to an integral which can be written in terms of elementary functions, whereas the contribution from the black hole leads to a more complicated integral which can be written in terms of the incomplete elliptic

integrals of the first and second kind,

$$I(R)\sigma_{\rm p}^2(R) = (1-\mu)\left[\frac{4R^2-1}{8R} - \frac{12R^2+1}{12\pi R^2} + \frac{3-4R^2}{4\pi}X(R)\right] + \frac{\mu}{105\pi}\left[\frac{5-96R^2}{R^2} + \frac{2(96R^2-17)\sqrt{R+1}}{R^{3/2}}\mathbb{E}\left(\frac{\pi}{4},\sqrt{\frac{2}{R+1}}\right) - \frac{192R^4-82R^2-5}{R^{5/2}\sqrt{R+1}}\mathbb{F}\left(\frac{\pi}{4},\sqrt{\frac{2}{R+1}}\right)\right], \tag{59}$$

with $X(R)$ a continuous real function defined as

$$X(R) = \begin{cases} \dfrac{1}{\sqrt{1-R^2}}\operatorname{arccosh}\left(\dfrac{1}{R}\right) & \text{if } R < 1, \\ \dfrac{1}{\sqrt{R^2-1}}\arccos\left(\dfrac{1}{R}\right) & \text{if } R > 1. \end{cases} \tag{60}$$

At large projected radii, the projected velocity dispersion profile behaves as

$$\sigma_{\rm p}^2(R) \approx \frac{8}{15\pi R}\left[1 - \frac{15\pi^2(4-\mu)-512}{128\pi R} + \cdots\right], \tag{61}$$

whereas at small projected radii we obtain

$$\sigma_{\rm p}^2(R) \approx \frac{\Gamma^2}{6\sqrt{2}\pi^{3/2}}\frac{1-\mu}{\sqrt{R}}\left[1 - \frac{3(8\pi^3-\Gamma^4)}{16\pi^2}R + \cdots\right] + \frac{\Gamma^4}{84\pi^2}\frac{\mu}{R}\left[1 - \frac{3(1344\pi^4-5\Gamma^8)}{\pi^2\Gamma^4}R + \cdots\right]. \tag{62}$$

In the first panel of Fig. 1 we plot the projected velocity dispersion profile for various values of the black hole mass. Notice that the projected velocity dispersion profile is nearly similar to the intrinsic dispersion profile. At a given projected radius R, the projected dispersion is a weighted mean of the dispersion along the line of sight. As the density is a strongly decreasing function of radius, stars around the tangent point $r \approx R$ will strongly dominate this mean, such that the projected velocity dispersion is nearly equal to the intrinsic dispersion at this point. As a result of this similarity, the effect of a black hole on the projected velocity dispersion is obviously similar to the effect on the intrinsic velocity dispersion. At large projected radii, there is obviously no effect from the black hole, whereas a black hole changes the slope of the projected dispersion profile at small projected radii from $-1/4$ to $-1/2$.

5 EXTENSION TO MODELS WITH AN ANISOTROPIC ORBITAL STRUCTURE

The models in the family we have described all have an isotropic dynamical structure, and consequently a distribution function $f(\mathcal{E})$ that depends only on the binding energy. General anisotropic distribution functions in spherically symmetric systems have distribution functions that depend on two integrals of motion, usually the binding energy and the modulus L of the angular momentum vector. The construction of general anisotropic dynamical models $f(\mathcal{E}, L)$ that correspond to a given spherical potential–density pair is discussed in detail by Dejonghe (1986). Also for anisotropic models, the key ingredient for the calculation of the distribution function and its moments is an augmented density. For anisotropic models, the augmented density is an explicit function of both radius and potential, i.e. a function $\tilde{\rho}(\Psi, r)$. For each potential–density pair, infinitely many of these augmented density functions and thus anisotropic dynamical models can be constructed. The only requirements are that the condition

$$\tilde{\rho}(\Psi(r), r) \equiv \rho(r) \tag{63}$$

is satisfied and that the corresponding distribution function is non-negative over the entire phase space. Unfortunately the formulae to calculate the distribution function and its moments from the augmented density are significantly more complicated than the Eddington formula (13) in the isotropic case. A number of different approaches exist, including for example, an approach with combined Laplace–Mellin transforms. There are a number of special cases, however, for which the construction of anisotropic dynamical models is not much more demanding than the construction of isotropic models. This has been illustrated by Baes & Dejonghe (2002), who constructed three different families of analytical dynamical models for the self-consistent Hernquist potential–density pair, with widely different dynamical structure. In this section we briefly describe how our family of isotropic dynamical models with a central black hole can be generalized to models with a constant anisotropy, models with an Osipkov–Merritt type distribution function and models with a completely radial orbital structure. Further generalizations, such as Cuddeford (1991) models, are also possible.

5.1 Models with a constant anisotropy

A special family of dynamical models corresponds to models with an augmented density $\tilde{\rho}(\Psi, r)$ that is a power law of r,

$$\tilde{\rho}(\Psi, r) = \tilde{\rho}_{\rm A}(\Psi) r^{-2\beta}, \tag{64}$$

where $\beta < 1$ and where the function $\tilde{\rho}_{\rm A}(\Psi)$ is determined by the condition (63). It is well-known that augmented densities of the form (64) correspond to models with a constant anisotropy (Dejonghe 1986; Binney & Tremaine 1987). The distribution function is a power law of the angular momentum, and can be found through an Eddington-like formula

$$f(\mathcal{E}, L) = \frac{2^\beta}{(2\pi)^{3/2}}\frac{L^{-2\beta}}{\Gamma(1-\beta)\Gamma(\frac{1}{2}+\beta)}\int_0^{\mathcal{E}}\frac{{\rm d}^2\tilde{\rho}_{\rm A}}{{\rm d}\Psi^2}\frac{{\rm d}\Psi}{(\mathcal{E}-\Psi)^{1/2-\beta}}. \tag{65}$$

To calculate the distribution function for the model defined by the potential–density pair (4)–(5), we can transform equation (65) to an integration with respect to a in the same way as in Section 3.2. We directly obtain

$$\tilde{\rho}_{\rm A}(a) = \frac{1}{8\pi}\frac{(a^2-1)^{4-2\beta}}{a^3}. \tag{66}$$

If β is a half-integer number, the integrand in formula (65) is a rational function of a, and if β is an integer number, the integrand is the product of a rational function and the square root of a quadratic term in a. The distribution functions can consequently be written in terms of elementary functions only for all integer and half-integer values of β. The radial and tangential velocity dispersions can be found through a formula similar to equation (9)

$$\sigma_r^2(r) = \frac{\sigma_\theta^2(r)}{1-\beta} = \frac{\sigma_\phi^2(r)}{1-\beta} = \frac{1}{\rho_{\rm A}(r)}\int_r^\infty \frac{M(r)\rho_{\rm A}(r)\,{\rm d}r}{r^2}. \tag{67}$$

These expressions can also be written in terms of elementary functions for all integer and half-integer values of β. Similarly, analytical expressions can be derived for all higher-order moments if β is an integer or half-integer number.

5.2 Osipkov–Merritt models

Osipkov (1979) and Merritt (1985) developed an inversion technique for another special class of spherical anisotropic dynamical models, namely models where the distribution function depends on energy and angular momentum only through the combination $Q \equiv \mathcal{E} - L^2/2r_{\rm a}^2$, with $r_{\rm a}$ the so-called anisotropy radius and under the assumption that $f(\mathcal{E}, L) = 0$ for $Q < 0$. Such models are characterized by an augmented density of the form

$$\tilde{\rho}(\Psi, r) = \left(1 + \frac{r^2}{r_{\rm a}^2}\right)^{-1}\tilde{\rho}_{\rm Q}(\Psi), \tag{68}$$

where the function $\tilde{\rho}_{\rm Q}(\Psi)$ is determined by the condition (63). The Osipkov–Merritt models have an anisotropy profile of the form $\beta(r) = r^2/(r^2 + r_{\rm a}^2)$, i.e. they are isotropic in the centre and become completely radially anisotropic at large radii. For the calculation of distribution functions for Osipkov–Merritt models, one can use a formula very similar to the Eddington formula,

$$f(\mathcal{E}, L) = \frac{1}{\sqrt{8}\pi^2}\int_0^Q \frac{{\rm d}^2\tilde{\rho}_{\rm Q}}{{\rm d}\Psi^2}\frac{{\rm d}\Psi}{\sqrt{Q-\Psi}}. \tag{69}$$

For the model we consider, we obtain

$$\tilde{\rho}_{\rm Q}(a) = \tilde{\rho}(a) + \frac{1}{8\pi r_{\rm a}^2}\frac{(a^2-1)^2}{a^3}. \tag{70}$$

The distribution function of the Osipkov–Merritt models can be calculated in a very similar way to the distribution function of the isotropic models. We find after some algebra

$$\begin{aligned} f(\mathcal{E}, L) = f(Q) + \frac{\sqrt{2}}{128\pi^3 r_{\rm a}^2}\Bigg[&\frac{\mathcal{X}_{\rm Q}(Q,\mu)\sqrt{Q}}{(2-\mu+Q)^4(1+\mu Q)} \\ &+\frac{3(1-\mu)(19-24\mu+16\mu^2-16Q+23\mu Q-4Q^2)}{(2-\mu+Q)^{9/2}}{\rm arctanh}\left(\frac{\sqrt{(2-\mu+Q)Q}}{1+Q}\right)\Bigg], \end{aligned} \tag{71}$$

where $f(Q)$ represents the isotropic distribution function (29) and $\mathcal{X}_{\rm Q}(Q, \mu)$ is a polynomial with integer coefficients

$$\mathcal{X}_{\rm Q}(Q,\mu) = (199-383\mu+264\mu^2-80\mu^3+16\mu^4) + (67+58\mu-189\mu^2+96\mu^3)Q + (14+7\mu-5\mu^2)Q^2 + 2(1-\mu)Q^3. \tag{72}$$

The velocity dispersions for the Osipkov–Merritt models can be found through the formula

$$\sigma_r^2(r) = \frac{\sigma_\theta^2(r)}{1-\beta(r)} = \frac{\sigma_\phi^2(r)}{1-\beta(r)} = \frac{1}{\rho_{\rm Q}(r)}\int_r^\infty \frac{M(r)\rho_{\rm Q}(r)\,{\rm d}r}{r^2}. \tag{73}$$

This integral can easily be evaluated analytically, and also the higher-order moments of the distribution function can be expressed completely in terms of elementary functions for all values of $r_{\rm a}$ and μ.

5.3 Models with a completely radial orbital structure

It deserves some special attention that the distribution function of both the models with constant anisotropy and the Osipkov–Merritt models corresponding to our potential–density pair (4)–(5) are positive for all values of β and $r_{\rm a}$ and for all values of the relative black hole mass μ. This is quite unusual. In the limit $r_{\rm a} \to 0$ or $\beta \to 1$ for the Osipkov–Merritt and constant-anisotropy models, respectively, the entire galaxy is populated with only radial orbits. Not all density profiles can sustain such a model: Richstone & Tremaine (1984) demonstrated that the density must diverge at least as r^{-2} at small radii in order to be able to sustain a purely radial orbital structure. Models with constant density cores or density cusps shallower than r^{-2} will hence have a minimal anisotropy radius $r_{\rm a,min}$ below which Osipkov–Merritt models are negative at some point in phase space, and a maximum anisotropy value $\beta_{\rm max}$ above which the constant-anisotropy models become negative at some point in phase space. For example, self-consistent Plummer models have $\beta_{\rm max} = 0$ and $r_{\rm a,min} = 3/4$ (Merritt 1985), and self-consistent Hernquist

models have $\beta_{\max} = 1/2$ and $r_{\mathrm{a,min}} \approx 0.202$ (Baes & Dejonghe 2002). The central slope of the density (4) for the models we consider in this paper is steep enough such that even models with a purely radial orbital structure are positive over the entire phase space.

For models with a completely radial orbital structure, the augmented density can be written as

$$\tilde{\rho}(\Psi, r) = \frac{\tilde{\rho}_{\mathrm{R}}(\Psi)}{r^2}, \tag{74}$$

where the function $\tilde{\rho}_{\mathrm{R}}(\Psi)$ is determined by the condition (63). The distribution function is of course a degenerate function of angular momentum (only orbits with $L = 0$ are populated), and can be calculated via the Eddington-like formula

$$f(\mathcal{E}, L) = \frac{\delta(L^2)}{\sqrt{2}\pi^2} \int_0^{\mathcal{E}} \frac{\mathrm{d}\tilde{\rho}_{\mathrm{R}}}{\mathrm{d}\Psi} \frac{\mathrm{d}\Psi}{\sqrt{\mathcal{E} - \Psi}}. \tag{75}$$

Once again, a closed expression can be obtained for the family of potential–density pairs we have discussed in this paper by transforming the integral to an integration with respect to the variable a. One obtains after some algebra

$$\begin{aligned} f(\mathcal{E}, L) = \frac{\sqrt{2}\delta(L^2)}{32\pi^3} \Bigg[&- \frac{(17 - 29\mu + 14\mu^2 - 3\mathcal{E} + 3\mu\mathcal{E} - 2\mathcal{E}^2)\sqrt{\mathcal{E}}}{(2 - \mu + \mathcal{E})^3} + \frac{2}{\sqrt{\mu}} \arctan\sqrt{\mu\mathcal{E}} \\ &+ \frac{(1-\mu)(1 - 4\mu - 2\mu^2 - 16\mathcal{E} - 17\mu\mathcal{E} + 4\mathcal{E}^2)}{(2 - \mu + \mathcal{E})^{7/2}} \operatorname{arctanh}\left(\frac{\sqrt{(2 - \mu + \mathcal{E})\mathcal{E}}}{1 + \mathcal{E}}\right) \Bigg]. \end{aligned} \tag{76}$$

This distribution function is everywhere positive, for all values of the black hole mass μ. The tangential velocity dispersions for these models are of course identically zero, whereas the radial velocity dispersion can be found through equation (67),

$$\sigma_r^2(r) = (1-\mu)\sqrt{\frac{1+r}{r}} \left(1 + 2r - 4r(1+r)\ln\sqrt{\frac{1+r}{r}}\right) + \frac{2\mu}{3}\left(\frac{1+r}{r}\right)\left(1 - 4r - 8r^2 + 8r^{3/2}\sqrt{1+r}\right). \tag{77}$$

6 CONCLUSION

We have described a one-parameter family of spherical models for elliptical galaxies and bulges consisting of a stellar component and a central black hole. All models in this family share the same stellar density profile, which has a steep cusp with a slope of $-5/2$ in the centre. The gravitational potential for the models is a linear combination of the potential generated self-consistently by the stars and the potential of a central supermassive black hole. The parameter μ, representing the mass of the black hole relative to the total mass of the galaxy, can assume any value between 0 and 1. The family therefore contains models ranging from a self-consistent model without a black hole to a model where the potential is entirely dominated by the black hole. We have done an extensive study of the internal and projected kinematics for this family of models. With the assumption of isotropy, we have calculated the intrinsic velocity dispersions, the distribution function, the differential energy distribution, the moments of the distribution function, the surface brightness and the projected velocity dispersions. All of these quantities have been expressed completely analytically, for all values of μ.

We have also described some extensions of the models to anisotropic orbital structures. In particular, we have considered models with a constant anisotropy, models with distribution functions of the Osipkov–Merritt type and models with a completely radial orbital structure. Also for these families of models, the distribution function and its moments can be calculated completely analytically for all values of the central black hole mass μ.

We are well aware that the stellar component we have considered does not completely represent the detailed structure of the centres of galaxies. First, it has a fairly steep density cusp, which is at the edge of the observed range in real elliptical galaxies (Lauer et al. 1995; Gebhardt et al. 1996). With such a steep cusp, much of the stellar mass is very centrally concentrated, resulting in an infinitely deep stellar potential well. The addition of a black hole potential to this stellar potential does not drastically change the global mass distribution, such that the effects of a black hole on the kinematical properties are probably quite conservative. For example, the distribution function is substantially, but not very drastically, affected by the presence of a black hole, whereas this effect is much stronger for γ-models with a less steep density cusp (see fig. 6 in Tremaine et al. 1994). The reason why we focused on the density profile (4), and not on one of the other members of the family of γ-models with a shallower central density cusp for example, is that the $\gamma = 5/2$ model is unique in the way that it yields a relatively simple expression of the augmented density in the presence of a central black hole. It is the only member of the family of γ-models where the distribution function, the differential energy distribution and the moments can be completely expressed in terms of elementary functions. We are currently undertaking a more general study of the properties of the γ-models with a central black hole, using both analytical and numerical means (Baes, Buyle & Dejonghe, in preparation).

Secondly, the models presented here are spherically symmetric and isotropic, whereas few elliptical galaxies are thought to be perfectly spherical. Observational studies suggest that a substantial fraction of elliptical galaxies are at least moderately triaxial (Franx, van Gorkom & de Zeeuw 1994; Tremblay & Merritt 1995; Bak & Statler 2000). The central regions of galaxies with a central black hole are generally believed to be roughly axisymmetric, however. Indeed, supermassive black holes drive the shapes of galaxies in triaxial haloes toward axisymmetry by stochastic diffusion, either globally (Gerhard & Binney 1985; Norman, May & van Albada 1985; Merritt & Quinlan 1998; Valluri & Merritt 1998; Wachlin & Ferraz-Mello 1998), or at least in the central regions (Holley-Bockelmann et al. 2001, 2002). Still, axisymmetric systems have a much larger freedom in orbital structure than spherical systems. Using detailed axisymmetric dynamical modelling, Gebhardt

et al. (2003) found that the central regions of the massive early-type galaxies generally have a significant tangential anisotropy, whereas less massive galaxies have a range of anisotropies.

In spite of these critical notes, the family of dynamical models presented in this paper has the huge advantage over more complicated numerical models that all kinematical properties can be calculated completely in terms of elementary functions, for any value of the parameter μ. This is not only the case for rather simple kinematical properties such as the velocity dispersions, but also for more complicated kinematical properties which depend in a strongly non-linear way on the potential. In particular, the distribution function and the differential energy distribution can be written in a compact form and in terms of elementary functions only. As a result, this family of models is useful for a large set of applications. In particular, it can be used to easily generate the initial conditions for N-body or hydrodynamical simulations, which are needed to investigate how black holes interact with the stellar, gaseous and dark matter components of their host galaxies.

ACKNOWLEDGMENT

MB is a Postdoctoral Fellow of the Fund for Scientific Research, Flanders, Belgium (F.W.O.-Vlaanderen). Part of this work was done in Cardiff, where MB was a visiting postdoctoral fellow. He gratefully acknowledges the hospitality of Cardiff University and the financial support of the Fund for Scientific Research Flanders. The authors thank the anonymous referee for useful suggestions that enhanced the content and presentation of the paper.

REFERENCES

Abramowitz M., Stegun I. A., 1972, Handbook of Mathematical Functions. Dover, New York
Baes M., Dejonghe H., 2002, A&A, 393, 485
Baes M., Buyle P., Hau G. K. T., Dejonghe H., 2003, MNRAS, 341, L44
Bak J., Statler T., 2000, AJ, 120, 110
Baumgardt H., Hut P., Makino J., McMillan S., Portegies Zwart S., 2003a, ApJ, 582, L21
Baumgardt H., Makino J., Hut P., McMillan S., Portegies Zwart S., 2003b, ApJ, 589, L25
Binney J., Tremaine S., 1987, Galaxy Dynamics. Princeton Univ. Press, Princeton
Cuddeford P., 1991, MNRAS, 253, 414
Ciotti L., 1996, ApJ, 471, 68
Cretton N., de Zeeuw P. T., van der Marel R. P., Rix H.-W., 1999, ApJS, 124, 383
Dejonghe H., 1986, Phys. Rep., 133, 217
Dejonghe H., 1987, MNRAS, 224, 13
Dejonghe H., 1989, ApJ, 343, 113
Dejonghe H., Mathieu A., De Bruyne V., De Rijcke S., 1999, Celest. Mech. Dyn. Astron., 72, 219
Dehnen W., 1993, MNRAS, 265, 250
Eddington A. S., 1916, MNRAS, 76, 572
Emsellem E., Monnet G., Bacon R., 1994, A&A, 285, 723
Ferrarese L., 2002, ApJ, 578, 90
Ferrarese L., Merritt D., 2000, ApJ, 539, L9
Franx M., van Gorkom J. H., de Zeeuw P. T., 1994, ApJ, 463, 642
Gebhardt K. et al., 1996, AJ, 112, 105
Gebhardt K. et al., 2000a, AJ, 119, 1157
Gebhardt K. et al., 2000b, ApJ, 539, L13
Gebhardt K., Rich M. R., Ho L. C., 2002, ApJ, 578, L41
Gebhardt K. et al., 2003, ApJ, 583, 92
Genzel R. et al., 2003, ApJ, 594, 812
Gerhard O. E., Binney J., 1985, MNRAS, 216, 467
Gerhard O., Jeske G., Saglia R. P., Bender R., 1998, MNRAS, 295, 197
Gerssen J., van der Marel R. P., Gebhardt K., Guhathakurta P., Peterson R. C., Pryor C., 2002, AJ, 124, 3270
Gerssen J., van der Marel R. P., Gebhardt K., Guhathakurta P., Peterson R. C., Pryor C., 2003, AJ, 125, 376
Ghez A. M., Morris M., Becklin E. E., Tanner A., Kremenek T., 2000, Nature, 407, 349
Graham A. W., Trujillo I., Caon N., 2001, AJ, 122, 1707
Hénon M., 1959, Ann. d'Astrophys., 22, 126
Hénon M., 1960, Ann. d'Astrophys., 23, 474
Hernquist L., 1990, ApJ, 356, 359
Holley-Bockelmann K., Mihos J. C., Sigurdsson S., Hernquist L., 2001, ApJ, 549, 862
Holley-Bockelmann K., Mihos J. C., Sigurdsson S., Hernquist L., Norman C., 2002, ApJ, 567, 817
Jaffe W., 1983, MNRAS, 202, 995
Kormendy J., Richstone D., 1995, ARA& A, 33, 581
Lauer T. R., Ajhar E. A., Byun Y., Dressler A., Faber S. M., 1995, AJ, 110, 2622
Marconi A., Hunt L. K., 2003, ApJ, 589, L21
McLure R. J., Dunlop J. S., 2002, MNRAS, 331, 795
McNamara B. J., Harrison T. E., Anderson J., 2003, ApJ, 595, 187
Merritt D., 1985, AJ, 90, 1027
Merritt D., Quinlan G., 1998, ApJ, 498, 625
Norman C. A., May A., van Albada T. S., 1985, ApJ, 296, 20

Osipkov L. P., 1979, Sov. Astron. Lett., 5, 42
Plummer H. C., 1911, MNRAS, 71, 460
Press W. H., Teukolsky S. A., Vetterling W. T., Brian P. F., 2001, Numerical Recipes in C++. Cambridge Univ. Press, Cambridge
Rix H.-W., de Zeeuw P. T., Cretton N., van der Marel R. P., Carollo C. M., 1997, ApJ, 488, 702
Ravindranath S., Ho L. C., Peng C. Y., Filippenko A. V., Sargent W. L. W., 2001, AJ, 122, 653
Richstone D. O., Tremaine S., 1984, ApJ, 286, 27
Saha P., 1993, MNRAS, 262, 1062
Salpeter E. E., 1964, ApJ, 140, 796
Schödel R. et al., 2002, Nat, 419, 694
Seigar M., Carollo C. M., Stiavelli M., de Zeeuw P. T., Dejonghe H., 2002, AJ, 123, 184
Soltan A., 1982, MNRAS, 200, 115
Tremaine S. et al., 2002, ApJ, 574, 740
Tremaine S. et al., 1994, AJ, 107, 634
Tremblay B., Merritt D., 1995, AJ, 110, 1039
Valluri M., Merritt D., 1998, ApJ, 506, 686
van der Marel R. P., Cretton N., de Zeeuw P. T., Rix H.-W., 1998, ApJ, 493, 613
Verolme E. K., de Zeeuw P. T., 2002, MNRAS, 331, 959
Wachlin F. C., Ferraz-Mello S., 1998, MNRAS, 298, 22
Zhao H., 1996, MNRAS, 278, 488

APPENDIX A: EVALUATION OF THE INCOMPLETE ELLIPTIC INTEGRALS

The expressions (51), (56) and (59) for the surface brightness, the cumulative surface brightness and the projected velocity dispersion contain incomplete elliptic integrals of the first and second kind. When the modulus of these functions (the second parameter) is less than unity, these functions are easily evaluated numerically, and simple and efficient routines are widely available (e.g. Press et al. 2001). Sophisticated closed-box mathematical packages such as MAPLE or MATHEMATICA easily calculate incomplete elliptic integrals for all (complex) values of the modulus, but most basic implementations break down when the modulus is greater than unity. For the present case, this happens when $R < 1$. A well-behaved solution for $R < 1$ can be obtained with the transformation formulae for incomplete elliptic integrals (e.g. Abramowitz & Stegun 1972). The relevant formulae to transform the expressions for the surface brightness profile, etc. for $R < 1$ are

$$\mathbb{F}\left(\frac{\pi}{4},\sqrt{\frac{2}{R+1}}\right)=\sqrt{\frac{R+1}{2}}\,\mathbb{F}\left(\arctan\sqrt{\frac{1}{R}},\sqrt{\frac{R+1}{2}}\right), \tag{A1}$$

$$\mathbb{E}\left(\frac{\pi}{4},\sqrt{\frac{2}{R+1}}\right)=\sqrt{\frac{2}{R+1}}\,\mathbb{E}\left(\arctan\sqrt{\frac{1}{R}},\sqrt{\frac{R+1}{2}}\right)+\frac{R-1}{\sqrt{2(R+1)}}\,\mathbb{F}\left(\arctan\sqrt{\frac{1}{R}},\sqrt{\frac{R+1}{2}}\right). \tag{A2}$$

Around $R = 1$ either of these forms are hard to evaluate numerically, because the modulus of the elliptic integrals then approaches unity. Instead, it is better to use the Taylor expansion

$$\mathbb{F}\left(\frac{\pi}{4},\sqrt{\frac{2}{R+1}}\right)\approx\frac{\ell}{\sqrt{2}}+\frac{\ell-2}{8\sqrt{2}}(R-1)-\frac{7\ell-26}{256\sqrt{2}}(R-1)^2+\cdots, \tag{A3}$$

$$\mathbb{E}\left(\frac{\pi}{4},\sqrt{\frac{2}{R+1}}\right)\approx\frac{1}{\sqrt{2}}+\frac{\ell-1}{4\sqrt{2}}(R-1)-\frac{5\ell-4}{64\sqrt{2}}(R-1)^2+\cdots, \tag{A4}$$

where

$$\ell=\frac{1}{\sqrt{2}}\operatorname{arctanh}\left(\frac{1}{\sqrt{2}}\right)=\frac{1}{2\sqrt{2}}\ln\left(\frac{\sqrt{2}-1}{\sqrt{2}+1}\right)\approx 0.62323. \tag{A5}$$

For example, for the surface brightness profile, we obtain

$$I(R)\approx\frac{1}{\pi}\left[\frac{5-7\ell}{8}-\frac{3(31-37\ell)}{128}(R-1)+\frac{1727-1797\ell}{2048}(R-1)^2-\cdots\right]. \tag{A6}$$

This paper has been typeset from a TEX/LATEX file prepared by the author.